THE JOURNAL OF BIOLOGICAL CHEMISTRY VOL. 286, NO. 4, pp. 2648–2657, January 28, 2011

HES1 (Hairy and Enhancer of Split 1) Is a Determinant of Bone Mass*

Received for publication, September 8, 2010, and in revised form, November 11, 2010 Published, JBC Papers in Press, November 17, 2010, DOI 10.1074/jbc.M110.183038

Stefano Zanotti[‡§1], **Anna Smerdel-Ramoya**[‡], **and Ernesto Canalis**[‡§]

From the [‡]*Department of Research, Saint Francis Hospital and Medical Center, Hartford, Connecticut 06105, and the* [§]*University of Connecticut School of Medicine, Farmington, Connecticut 06030*

HES1 (hairy and enhancer of split) is a transcription factor that regulates osteoblastogenesis *in vitro*. The skeletal effects of HES1 misexpression were studied. Transgenic mice where a 3.6-kilobase fragment of the collagen type 1 α1 promoter directs HES1 overexpression were created. Transgenics were osteopenic due to decreased osteoblast function in female and increased bone resorption in male mice. HES1 impaired osteoblastogenesis *in vitro*, and transgenic osteoblasts enhanced the resorptive activity of co-cultured osteoclast precursors. Mice homozygous for a *Hes1 loxP*-targeted allele were bred to transgenics, where the paired-related homeobox gene enhancer or the osteocalcin promoter direct Cre recombinase expression to inactivate *Hes1* in the limb bud or in osteoblasts. To avoid genetic compensation, *Hes1* was inactivated in the context of the global deletion of *Hes3* and *Hes5*. *Hes3* and *Hes5* null mice had no skeletal phenotype. *Hes1* inactivation in the limb bud increased femoral length and trabecular number. *Hes1* inactivation in osteoblasts increased trabecular bone volume, number, and connectivity due to increased mineral apposition rate and suppressed bone resorption. *Hes1* inactivation *in vitro* increased alkaline phosphatase expression and suppressed the resorptive activity of co-cultured osteoclast precursors. In conclusion, by inhibiting osteoblast function and inducing bone resorption, HES1 is an intracellular determinant of bone mass and structure.

HES is a family of evolutionary conserved basic helix-loop-helix transcription factors that comprises seven members, termed HES1 through HES7 (1–4). HES proteins are homologues of *Drosophila Hes* and were first identified as targets of canonical Notch signaling. Notch signaling is activated following cell to cell contact interactions and is critical for developmental processes and the regulation of tissue renewal and maintenance (5–9). HES proteins generally act as repressors of transcription (3). HES1, -3, and -5 have partially overlapping functions, are involved in binary cell fate decisions, and maintain precursor multipotent cells in an undifferentiated state in several tissues during development and adult life (3, 10–13). HES1 is necessary for neural development, and its global inactivation results in early embryonic or perinatal lethality (14).

Bone remodeling is a process carried out in discrete multicellular units, where osteoclasts resorb bone and osteoblasts form new bone in a coordinated fashion to renew skeletal tissue (15). Osteoblasts are derived from multipotent bone marrow mesenchymal stem cells, whereas osteoclasts are derived from multipotent hematopoietic cells (16). Bone marrow mesenchymal stem cells can differentiate toward the osteoblastic, chondrocytic, and adipocytic lineages (17). The fate of mesenchymal cells and their differentiation into osteoblasts is controlled by a signaling network that includes bone morphogenetic proteins, Wnt and Notch (18–23). Notch signaling inhibits osteoblast differentiation and causes osteopenia *in vivo*, but even though HES1 is a target of Notch, it does not recapitulate all of the effects of Notch (24). HES1 participates in cell fate determination of mesenchymal multipotent cells and blocks the initial differentiation of preadipocytes, although it is necessary for their terminal differentiation (25, 26). HES1 suppresses the expression of osteocalcin and induces the transcription of osteopontin (27, 28). In addition, HES1 interacts with RUNX2 (runt-related transcription factor 2) prolonging its half-life, and, as a consequence, enhances the differentiation of murine osteoblastic cells (28–31). However, the function of HES1 in skeletal tissue has not been established.

Osteoclasts are multinucleated cells that form through the aggregation of bone marrow mononuclear cell precursors. Osteoclast formation requires RANKL (receptor activator of NF-κB ligand), a membrane-bound ligand of RANK, and its activity is opposed by the soluble decoy receptor osteoprotegerin (32, 33). RANKL and osteoprotegerin are expressed by bone marrow stromal cells and osteoblasts, and their ratio regulates osteoclastogenesis. Notch signaling inhibits the maturation of bone marrow osteoclast precursors by inducing the expression of osteoprotegerin (21, 34, 35). However, the role of HES1 in osteoclastogenesis is not known.

The intent of this study was to define the function of HES1 on skeletal development and postnatal bone remodeling. For this purpose, transgenic mice overexpressing HES1 under the control of a 3.6-kb rat collagen type 1 α1 (*Col1a1*) promoter fragment were created. In addition, a conditional deletion approach to ablate *Hes1* in the skeleton and avoid the lethality of the global *Hes1* inactivation was employed (14). Mice, where *Hes1* sequence coding exons were flanked by *loxP* sequences ($Hes1^{loxP/loxP}$), were bred to transgenics expressing the Cre recombinase under the control of the paired-related

* This work was supported, in whole or in part, by National Institutes of Health Grant DK045227 from the NIDDK.

[1] To whom correspondence should be addressed: Dept. of Research, Saint Francis Hospital and Medical Center, 114 Woodland St., Hartford, CT 06105-1299. Tel.: 860-714-5250; Fax: 860-714-8053; E-mail: szanotti@stfranciscare.org.

homeobox 1 (*Prx1*) enhancer (*Prx1-Cre*) or the osteocalcin promoter (*Oc-Cre*), to inactivate *Hes1* in the limb bud or in mature osteoblasts, respectively. *Hes1* conditional null mice were created in a *Hes3* and *Hes5* null background ($Hes3^{-/-}$ $Hes5^{-/-}$), to avoid a possible phenotypic compensation following the inactivation of *Hes1*. The skeletal phenotype of mice misexpressing HES1 was studied by histomorphometric and structural analysis of the femur. To understand the mechanisms of HES1 action in bone, the differentiation and function of skeletal cells misexpressing HES1 were examined *in vitro*.

EXPERIMENTAL PROCEDURES

Hes1 Transgenic Mice—After introduction of a Kozak consensus sequence upstream of the translation initiation codon, a 1.5-kb cDNA fragment coding for murine HES1 was cloned downstream of the 3.6-kb fragment of the rat *Col1a1* promoter and upstream of the bovine growth hormone polyadenylation signal (36). Microinjection of linearized DNA into pronuclei of fertilized oocytes from Friend leukemia virus strain B (FVB) inbred mice (Charles River Laboratories, Wilmington, MA), and transfer of microinjected embryos into pseudopregnant mice were carried out at the Gene Targeting and Transgenic Facility of the University of Connecticut Health Center (Farmington, CT). Positive founders were identified by Southern blot analysis of tail DNA and bred to wild type FVB mice to create transgenic lines (37). Heterozygous transgenic mice were mated to wild type FVB mice to generate heterozygous HES1 transgenic mice and wild type littermate controls for the experiments described. Presence of the *Hes1* transgene was documented by PCR in tail DNA (Table 4).

Hes1 Conditional Null Mice—Mice where the *Hes1* sequence comprised between exons 2 and 4 was flanked by *loxP* sequences and deletion mutant mice for *Hes3* and *Hes5*, created in a CD1 genetic background, were obtained from R. Kageyama (Kyoto University, Kyoto, Japan) (38–40). $Hes1^{loxP/loxP}$ mice were bred to $Hes3^{-/-}$;$Hes5^{-/-}$ to create $Hes1^{loxP/loxP}$;$Hes3^{-/-}$;$Hes5^{-/-}$ mice. To study the consequences of the inactivation of *Hes1* during early limb development, *Prx1-Cre* mice created in a C57BL/6 genetic background, were obtained from The Jackson Laboratory (Bar Harbor, ME) (41). To study the inactivation of *Hes1* in mature osteoblasts, transgenic mice expressing the Cre recombinase under the control of a 3.9 kb human osteocalcin promoter, created in an FVB genetic background, were obtained from T. Clemens (Baltimore, MD) (42). Transgenics expressing Cre were bred to $Hes1^{loxP/loxP}$;$Hes3^{-/-}$;$Hes5^{-/-}$ mice to create heterozygous *Prx1-Cre*/+;$Hes1^{loxP/+}$;$Hes3^{+/-}$;$Hes5^{+/-}$ or *Oc-Cre*/+;$Hes1^{loxP/+}$;$Hes3^{+/-}$;$Hes5^{+/-}$ mice. These were mated with $Hes1^{loxP/loxP}$;$Hes3^{-/-}$;$Hes5^{-/-}$ to create *Prx1-Cre*/+;$Hes1^{loxP/loxP}$;$Hes3^{-/-}$;$Hes5^{-/-}$ and *Oc-Cre*/+;$Hes1^{loxP/loxP}$;$Hes3^{-/-}$;$Hes5^{-/-}$. These mice were mated with $Hes1^{loxP/loxP}$;$Hes3^{-/-}$;$Hes5^{-/-}$ to generate an experimental cohort, in which Cre excises the *loxP*-flanked sequences from the $Hes1^{loxP}$ allele ($Hes1^{\Delta/\Delta}$;$Hes3^{-/-}$;$Hes5^{-/-}$) and a control littermate group ($Hes1^{loxP/loxP}$;$Hes3^{-/-}$;$Hes5^{-/-}$). Male and female conditional null mice were compared with littermate controls of the same sex at 15 and 18 days post coitum, at birth, and at 1, 3, and 6 months of age, and their skeletal phenotype was analyzed. To ensure the validity of $Hes1^{loxP/loxP}$;$Hes3^{-/-}$;$Hes5^{-/-}$ mice as controls, the skeletal phenotype of $Hes3^{-/-}$;$Hes5^{-/-}$ mice was compared with that of wild type littermates, and the phenotype of $Hes1^{loxP/loxP}$;$Hes3^{-/-}$;$Hes5^{-/-}$ mice was compared with that of $Hes3^{-/-}$;$Hes5^{-/-}$ littermates at 1 month of age. Detection of $Hes1^{loxP}$, $Hes3^{-}$, and $Hes5^{-}$ alleles was carried out by PCR in tail DNA extracts in newborns and adult mice (Table 1). Excision of *loxP*-flanked sequences by Cre recombinase was documented by PCR in DNA extracted from calvariae of 1-, 3-, and 6-month-old mice, using specific primers (Table 1). All animal experiments were approved by the Animal Care and Use Committee of Saint Francis Hospital and Medical Center.

TABLE 1
Primers used for genotyping by PCR and for mRNA level determination by real-time RT-PCR
[FAM] indicates the position of the guanine labeled with the fluorophore.

Primers for genotyping			
Allele	**Strand**	**Primer Sequence**	**Size (bp)**
Hes1 transgene	Forward	5'-GAGCAGGAGGCACACGGA-3'	500
	Reverse	5'-GGACAGGAAGCGGGTCAC-3'	
$Hes1^{loxP}$	Forward	5'-CAGCCAGTGTCAACACGACACCGGACAAAC-3'	313 $Hes1^{+}$
	Reverse1	5'-GGTGGGGCTTGAAATTCATGTTTGGC-3'	360 $Hes1^{loxP}$
	Reverse2	5'-CCTGAGTAAGGACAGACAAATGAAGGTCC-3'	330 $Hes1^{\Delta}$
$Hes3^{-}$	Forward	5'-GGCGGGCTGCACGCTTTAATGGGACACATG-3'	450 $Hes3^{+}$ 840 $Hes3^{-}$
	Reverse1	5'-CAGTATGTCTGCTTGCCAAGTCCTGGCTGC-3'	
	Reverse2	5'-ATTACGCCAGCTGGCGAAAGGgGGATGTGC-3'	
$Hes5^{-}$	Forward	5'-CCAGCCCAACTCCAAGCTGGAGAAGGC-3'	200 $Hes5^{+}$ 600 $Hes5^{-}$
	Reverse1	5'-CAGGAGTAGCCCTCGCTGTAGTCCTGG-3'	
	Reverse2	5'-GGGCTGACCGCTTCCTCGTGCTTTACG-3'	
Primers for real time RT-PCR			
Gene	**Strand**	**Primer Sequence**	
Alkaline phosphatase	Forward	5'-CGGTTAGGGCGTCTCCACAGTAAC[FAM]G-3'	
	Reverse	5'-CTTGGAGAGGGCCACAAAGG-3'	
Hes1	Forward	5'-GACTTTCACGGCCTCTGAGCACAGAAAG[FAM]C-3'	
	Reverse	5'-ATTCTTGCCCTTCGCCTCTT-3'	
Osteocalcin	Forward	5'-CACTTACGGCGCTACCTTGGGTAAGT[FAM]G-3'	
	Reverse	5'-CCCAGCACAACTCCTCCCTA-3'	
Rpl38	Forward	5'-CGAACCGGATAATGTGAAGTTCAAGGTT[FAM]G-3'	
	Reverse	5'-CTGCTTCAGCTTCTCTGCCTTT-3'	

X-ray Analysis, BMD, and Femoral Length—X-Rays were performed on eviscerated mice at an intensity of 30 kW for 20 s on a Faxitron X-Ray system (model MX 20, Faxitron X-Ray Corp., Wheeling, IL). Total bone mineral density (BMD[2]; g cm^{-2}) was measured on anesthetized mice using the PIXImus small animal DEXA system (GE Medical System/LUNAR, Madison, WI) (43). Femoral images were used to determine femoral length (mm). Calibrations were performed with a phantom of defined value, and quality assurance measurements were performed before each use. The coefficient of variation for total BMD is $<1\%$.

Bone Histomorphometric Analysis—Static and dynamic histomorphometry of femurs was carried out after injection with 20 mg/kg calcein and 50 mg/kg demeclocycline, at an interval of 2 days for 1-month-old mice and 7 days for 3- and

[2] The abbreviations used are: BMD, bone mineral density; Col1a1, collagen type 1 α1; FVB, Friend leukemia virus strain B; Prx, paired-related homeobox gene; Rpl38, ribosomal protein L38.

6-month-old mice. Animals were sacrificed by CO_2 inhalation 2 days after the demeclocycline injection. Femoral longitudinal sections, 5-μm thick, were cut on a microtome (Microm, Richards-Allan Scientific, Kalamazoo, MI) and stained with 0.1% toluidine blue or von Kossa. Static parameters of bone formation and resorption were measured in a defined area between 360 and 2160 μm from the growth plate, using an OsteoMeasure morphometry system (Osteometrics, Atlanta, GA) (44). For dynamic histomorphometry, mineralizing surface per bone surface and mineral apposition rate were measured on unstained sections under ultraviolet light, using a triple diamino-2-phenylindole fluorescein set long pass filter, and bone formation rate was calculated. The terminology and units used are those recommended by the Histomorphometry Nomenclature Committee of the American Society for Bone and Mineral Research (45).

Microcomputed Tomography—Femurs were scanned using a Microcomputed Tomographic Instrument (μCT 40, Scanco Medical AG, Bassersdorf, Switzerland), calibrated weekly using a phantom provided by the manufacturer. Femurs were scanned in 70% ethanol at an energy level of 55 peak kilo voltage, intensity of 145 μA, and integration time of 200 ms. Trabecular bone volume and microarchitecture were evaluated starting ~1.2 mm proximal to the femoral condyles. A total of 160 consecutive slices acquired at an isotropic voxel size of 6 μm^3 and a slice thickness of 6 μm, were chosen for analysis. Contours were manually drawn every 10 slices a few voxels away from the endocortical boundary to define the region of interest for analysis. The contours of the remaining slices were iterated automatically. Trabecular regions were assessed for bone volume fraction, trabecular thickness, number and separation, connectivity density, and structural model index, using a Gaussian filter ($\sigma = 0.8$, support = 1) and a user-defined threshold (46). A total of 100 slices for the cortical region were measured at the mid-diaphysis of each femur with an isotropic voxel size of 6 μm^3 and a slice thickness of 6 μm. For mid-diaphysis analysis, contours were iterated across the 100 slices along the cortical shell, excluding the bone marrow cavity. Analysis for cortical thickness was performed using a Gaussian filter ($\sigma = 0.8$, support = 1) and a user-defined threshold (46).

Osteoblastic Cell Cultures—Primary osteoblasts were isolated from parietal bones of 3- to 5-day-old mice by sequential collagenase digestion, as described (47). Cells were cultured in DMEM (Invitrogen) supplemented with nonessential amino acids, 20 mM HEPES, 100 μg/ml ascorbic acid, and 10% FBS (Atlanta Biologicals, Norcross, GA) at 37 °C in a humidified 5% CO_2 incubator. Primary bone marrow stromal cells were recovered by centrifugation of femurs that were aseptically removed from 4-week-old HES1 transgenic and littermate control mice, as described (44). Cells were cultured in α-minimum essential medium (Invitrogen) containing 15% FBS at 37 °C in a humidified 5% CO_2 incubator.

Osteoblast-Splenocyte Co-cultures and Pit Formation Assay—Primary osteoblasts were seeded on BioCoat discs (BD Biosciences), and after reaching confluence, cultured in the presence of 100 μg/ml ascorbic acid and 5 mM β-glycerophosphate. Primary splenocytes were harvested from spleens aseptically removed from 5- to 8-week-old wild type FVB mice, and 1×10^6 cells/cm^2 were seeded on the layer of primary osteoblasts in the presence of 10 nM 1,25-dihydroxyvitamin D_3 (BIOMOL Intl., Plymouth Meeting, PA) or PBS, as control (48–50). Splenocytes and primary osteoblasts were cultured for 7 days; the cells were removed with bleach for 5 min, and BioCoat discs were stained with von Kossa. Discs were photographed on a white light background, and the digital image was analyzed with Adobe Photoshop (Adobe Systems, Inc., San Jose, CA). Brightness and contrast were maximized, the file was inverted to yield the negative image, and the area of resorption was calculated as the percent of pixels contained in half of the grayscale, determined by using the histogram function of Adobe Photoshop.

Real-time RT-PCR—Total RNA was extracted from cultures of primary osteoblastic cells, and mRNA levels were determined by real-time RT-PCR (51, 52). For this purpose, 1–3 μg of total RNA were reverse-transcribed using the SuperScript III Platinum Two-step Quantitative RT-PCR kit (Invitrogen), according to the manufacturer's instructions and amplified in the presence of specific primers (Table 1) and Platinum Quantitative PCR SuperMix-UDG (Invitrogen) at 60 °C for 30 cycles. The copy number was estimated by comparison with a standard curve constructed using alkaline phosphatase and HES1 (both from ATCC, Manassas, VA) and osteocalcin (from J. B. Lian, University of Massachusetts, Worcester, MA) cDNAs and corrected for ribosomal protein L38 (Rpl38; ATCC) expression (53–55). Reactions were conducted in a 96-well spectrofluorometric thermal iCycler (Bio-Rad), and fluorescence was monitored during every PCR cycle at the annealing step. Data are expressed as the copy number corrected for *Rpl38*.

Statistical Analysis—Data are expressed as means ± S.E. Statistical differences were determined by analysis of variance or Student's *t* test.

RESULTS

HES1 Overexpression Causes Osteopenia—Two transgenic lines overexpressing HES1 under the control of the 3.6-kb rat *Col1a1* promoter were established. Transgenic mice from both lines were osteopenic, and one line was studied in detail. Following heterozygous intermatings, only heterozygous transgenics were born, suggesting intrauterine lethality of homozygous transgenics. Therefore, heterozygous HES1 transgenic mice were used for subsequent analysis. These mice developed normally but did not live beyond 3 months of age; consequently, the analysis of their skeletal phenotype was performed in 1- and 3-month-old animals.

At 1 month of age, HES1 transgenics appeared normal, and no skeletal abnormalities were detected by contact radiography. Similarly, bone histomorphometric and microarchitectural analysis of 1-month-old transgenics did not reveal differences from littermate controls. HES1 transgenic mice at 3 months of age did not exhibit skeletal abnormalities by contact radiography and had normal BMD. However, transgenics of both sexes had significantly lower weight, and female transgenics displayed shortened femoral length (Fig. 1*A*). Bone histomorphometric analysis revealed a 20–25% decrease in

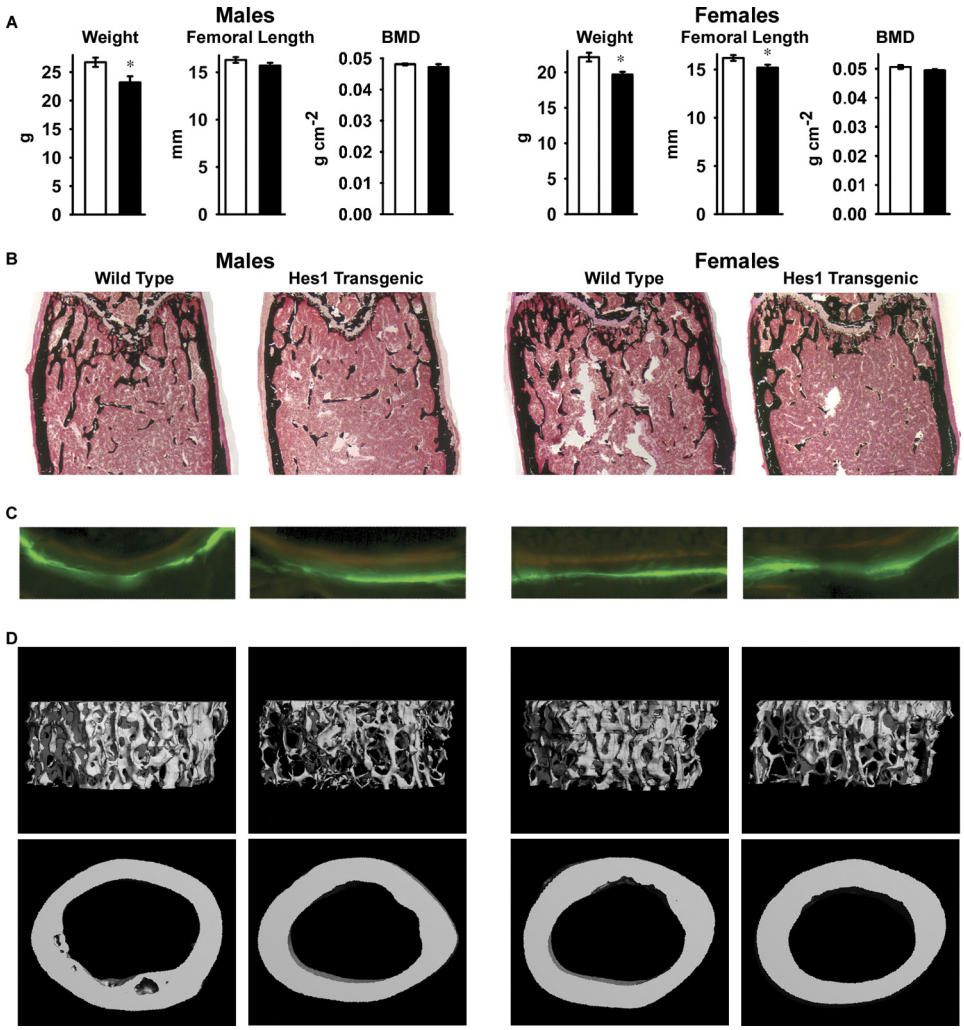

FIGURE 1. **Skeletal phenotype of 3-month-old male (*left*) and female (*right*) heterozygous HES1 transgenic mice (*black bars*) and wild type littermate controls (*white bars*).** In *A*, the weight (g), femoral length (mm), and total BMD (g cm^{-2}) are shown. Values are means ± S.E., $n = 6–8$. *, Significantly different from control mice, $p < 0.05$. Shown in *B* and *C* are von Kossa staining (*B*; final magnification, 40×) and calcein/demeclocycline labeling (*C*; final magnification, 100×) of representative femoral sections. *D*, microcomputed tomography of representative femurs.

trabecular bone volume, secondary to a reduced number of trabeculae, demonstrating that HES1 overexpression causes osteopenia (Table 2 and Fig. 1*B*). Although transgenics from both sexes were osteopenic, the mechanisms responsible appeared to be different. In male transgenics, there was a modest increase in the number of osteoclasts, leading to an increase in eroded surface, whereas in female transgenics, there was a decrease in osteoblast number associated with reduced osteoid surface. Bone formation and mineral apposition rate were not affected in either sex (Table 2 and Fig. 1*C*). Microcomputed tomography confirmed the decrease in trabecular bone volume, number, and increased separation observed by bone histomorphometry and revealed decreased connectivity density in HES1 transgenics of both sexes. Measurement of the structural model index revealed a higher ratio of rod-shaped *versus* plate-like trabeculae in HES1 transgenics. There were no differences in cortical bone thickness between transgenics and controls (Table 2 and Fig. 1*D*). These results indicate that overexpression of HES1 directed by a 3.6-kb *Col1a1* promoter fragment has a negative effect on trabecular microarchitecture without affecting cortical bone.

HES1 Overexpression Impairs Osteoblastogenesis and Induces Osteoclastogenesis in Vitro—To understand the mechanisms responsible for the effects of HES1 overexpression, calvarial osteoblasts and bone marrow stromal cells were harvested from HES1 transgenics and from wild type littermate controls of both sexes. HES1 transcripts were increased in primary osteoblastic cells from HES1 transgenics throughout the culture period, and calvarial osteoblasts expressed decreased levels of alkaline phosphatase and osteocalcin mRNA after 7 days of culture (Fig. 2*A*). In accordance with the results obtained in osteoblasts, alkaline phosphatase and osteocalcin mRNA levels were suppressed in transgenic bone marrow stromal cells after 7 days of culture (Fig. 2*B*). These findings confirm that HES1 overexpression impairs osteoblast differentiation and could explain the decreased number of osteoblasts observed in female HES1 transgenics.

To ascertain whether the overexpression of HES1 in osteoblasts increased osteoclast differentiation or function, calvarial osteoblasts from HES1 transgenics or wild type littermate controls of both sexes were co-cultured with splenocytes from wild type FVB mice, as a source of mononuclear oste-

TABLE 2

Femoral histomorphometry and bone microarchitecture of 3-month-old male and female HES1 transgenic mice and wild type controls

Femoral histomorphometry and microcomputed tomography were performed on femurs from 3-month-old male and female heterozygous HES1 transgenic mice and littermate wild type controls. Values are means ± S.E.; $n = 3–8$.

	Males		Females	
	Wild type	HES1	Wild type	HES1
Histomorphometry				
Bone volume/tissue volume (%)	7.1 ± 0.4	5.5 ± 0.6[a]	7.9 ± 0.6	5.8 ± 0.4[a]
Trabecular separation (μm)	268 ± 6	362 ± 41[a]	254 ± 14	337 ± 16[a]
Trabecular no. (mm^{-1})	3.5 ± 0.1	2.8 ± 0.3[a]	3.7 ± 0.2	2.8 ± 0.1[a]
Trabecular thickness (μm)	20.3 ± 0.9	19.7 ± 0.4	21.4 ± 0.9	20.2 ± 0.7
Osteoblast surface/bone surface (%)	11.0 ± 0.8	13.6 ± 1.7	13.7 ± 1.0	8.9 ± 1.3[a]
No. of osteoblasts/bone perimeter (mm^{-1})	12.5 ± 0.9	15.7 ± 2.0	14.8 ± 1.0	10.5 ± 1.2[a]
Osteoid surface/bone surface (%)	0.8 ± 0.3	0.7 ± 0.3	1.7 ± 0.3	0.5 ± 0.2[a]
Osteoclast surface/bone surface (%)	10.4 ± 0.3	11.6 ± 0.3[a]	13.3 ± 0.5	13.6 ± 0.6
No. of osteoclasts/bone perimeter (mm^{-1})	5.3 ± 0.1	6.0 ± 0.2[a]	6.9 ± 0.3	6.9 ± 0.3
Eroded surface/bone surface (%)	18.5 ± 0.6	20.8 ± 0.9[a]	23.9 ± 0.9	23.5 ± 1.2
Mineral apposition rate ($\mu m\ day^{-1}$)	0.63 ± 0.03	0.61 ± 0.03	0.82 ± 0.04	0.85 ± 0.06
Mineralizing surface/bone surface (%)	11.2 ± 0.8	12.8 ± 1.0	8.9 ± 1.0	9.0 ± 1.3
Bone formation rate ($\mu m^2\ \mu m^{-3}\ day^{-1}$)	0.071 ± 0.006	0.077 ± 0.005	0.073 ± 0.008	0.077 ± 0.013
Microcomputed tomography				
Bone volume fraction (%)	11.8 ± 0.7	7.6 ± 0.6[a]	13.9 ± 1.0	10.4 ± 0.8[a]
Trabecular separation (μm)	199 ± 3	242 ± 8[a]	215 ± 5	241 ± 8[a]
Trabecular no. (mm^{-1})	4.9 ± 0.1	4.1 ± 0.1[a]	4.7 ± 0.1	4.2 ± 0.1[a]
Trabecular thickness (μm)	37 ± 1	37 ± 1	42 ± 1	41 ± 1
Connectivity density (mm^{-3})	280 ± 16	138 ± 17[a]	267 ± 15	181 ± 17[a]
Structure model Index	2.0 ± 0.1	2.4 ± 0.1[a]	1.6 ± 0.1	2.0 ± 0.1[a]
Cortical thickness (μm)	179 ± 2	186 ± 4	199 ± 3	200 ± 2

[a] Significantly different from wild type controls, $p < 0.05$.

oclast precursors. Osteoclast activity was determined by the pit formation assay in a BD BioCoat cell culture system. Treatment with 1,25-dihydroxyvitamin D_3 enhanced the resorptive activity of wild type splenocytes (48). In accordance with the increased number of osteoclasts and eroded surface observed in male HES1 transgenics, osteoblasts from HES1 transgenics enhanced resorption in comparison to control osteoblasts. The effect was present whether the cultures were treated or not with 1,25-dihydroxyvitamin D_3 (Fig. 2*C*). These results indicate that HES1 overexpression in osteoblasts increases bone resorption and offer an explanation for the resorptive phenotype observed in male HES1 transgenics.

Controls for the Hes1 Conditional Null Mouse Model—The conditional inactivation of *Hes1* was studied in the context of the global ablation of *Hes3* and *Hes5* to prevent possible compensatory effects from HES3 and HES5 because they are expressed by osteoblasts, and their function partially overlaps with that of HES1 (3, 10, 12). One-month-old $Hes3^{-/-}$;$Hes5^{-/-}$ mice appeared normal and bone histomorphometry did not reveal differences between $Hes3^{-/-}$;$Hes5^{-/-}$ mice and wild type sex-matched littermates. To assess whether the presence of *loxP* sequences caused a skeletal phenotype, 1-month-old $Hes1^{loxP/loxP}$;$Hes3^{-/-}$;$Hes5^{-/-}$ mice were compared with $Hes3^{-/-}$;$Hes5^{-/-}$ sex-matched littermates. Absence of spontaneous recombination of the $Hes1^{loxP}$ allele was documented by PCR in calvarial extracts, and $Hes1^{loxP/loxP}$;$Hes3^{-/-}$;$Hes5^{-/-}$ mice were not different from $Hes3^{-/-}$;$Hes5^{-/-}$ mice when assessed by bone histomorphometry. These results indicate that $Hes1^{loxP/loxP}$;$Hes3^{-/-}$;$Hes5^{-/-}$ mice are valid controls for $Hes1^{\Delta/\Delta}$;$Hes3^{-/-}$;$Hes5^{-/-}$ experimental mice.

Inactivation of Hes1 in Limb Bud Mesenchyme Increases Bone Volume—To induce the conditional deletion of *Hes1* in the limb bud starting at day 10.5 of embryonic life, *Prx1-Cre*/+;$Hes1^{loxP/loxP}$;$Hes3^{-/-}$;$Hes5^{-/-}$ mice were mated with $Hes1^{loxP/loxP}$;$Hes3^{-/-}$;$Hes5^{-/-}$ mice to create *Prx1-Cre*/+;$Hes1^{\Delta/\Delta}$;$Hes3^{-/-}$;$Hes5^{-/-}$ conditional null and $Hes1^{loxP/loxP}$;$Hes3^{-/-}$;$Hes5^{-/-}$ littermate controls (41). The skeletal phenotype was investigated in 15- and 18-day-old embryos, newborns, and 1-month-old mice. Skeletal staining of embryos and newborn mice with alcian blue and alizarin red did not reveal obvious differences between *Hes1* conditional null mice and controls in cartilage and mineralized tissue (data not shown).

Recombination of $Hes1^{loxP}$ was documented in calvarial DNA extracts from 1-month-old *Prx1-Cre*/+;$Hes1^{\Delta/\Delta}$;$Hes3^{-/-}$;$Hes5^{-/-}$ mice (Fig. 3*A*). One-month-old conditional null mice appeared normal and contact radiography did not reveal differences when compared with littermate controls (data not shown). *Hes1* conditional null male mice exhibited increased femoral length and total BMD, indicating that *Hes1* inhibits longitudinal bone growth (Fig. 3*B*). Bone histomorphometric analysis of 1-month-old male *Hes1* conditional null mice revealed a 70% increase in trabecular bone volume that was secondary to an increased number of trabeculae (Table 3 and Fig. 3*C*). The osteoblast and osteoclast numbers were not changed, and no differences were observed in parameters of osteoblast or osteoclast function, suggesting that *Hes1* inactivation in the limb bud does not affect postnatal bone remodeling (Table 3 and Fig. 3*D*). The results from histomorphometric analysis were confirmed by microcomputed tomography. *Prx1-Cre*/+;$Hes1^{\Delta/\Delta}$;$Hes3^{-/-}$;$Hes5^{-/-}$ male mice exhibited a tendency toward increased bone volume fraction ($p < 0.065$) and a significant increase in connectivity density and trabecular number coupled to a decrease in trabecular separation, whereas cortical thickness was not affected (Table 3 and Fig. 3*E*). The phenotype was restricted to male mice, and $Hes1^{\Delta/\Delta}$;$Hes3^{-/-}$;$Hes5^{-/-}$ fe-

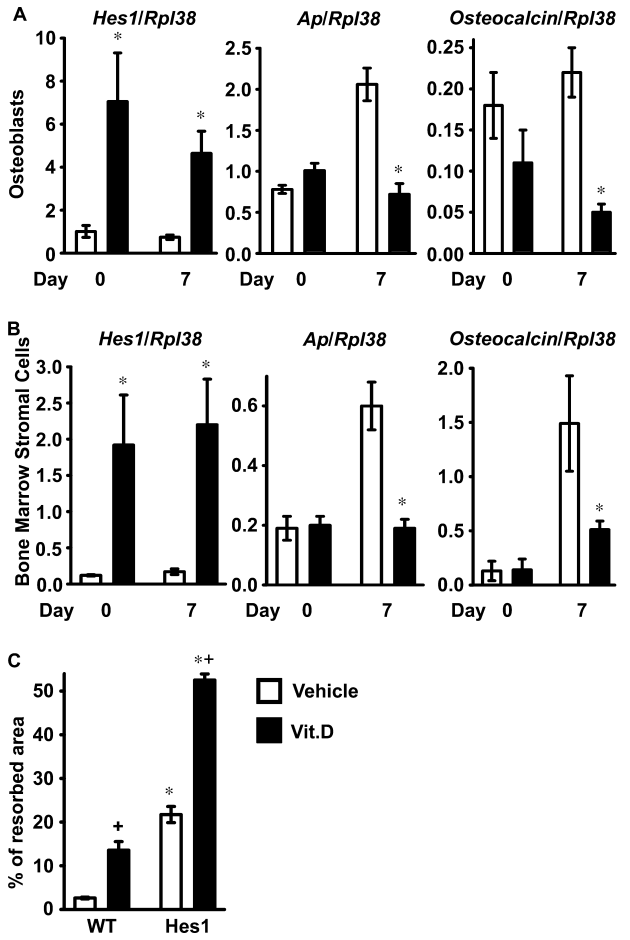

FIGURE 2. **Effects of HES1 overexpression on osteoblastic function *in vitro*.** In *A* and *B*, calvarial osteoblasts (*A*) and bone marrow stromal cells (*B*) were harvested from HES1 transgenics (*black bars*) and wild type littermate controls (*white bars*). Total RNA was extracted at confluence and after 7 days of culture in conditions favoring osteoblastogenesis; mRNA was reverse-transcribed and amplified by real time RT-PCR in the presence of specific primers. Data are expressed as *Hes1*, alkaline phosphatase (*Ap*), and osteocalcin copy number, determined by real time RT-PCR, corrected for *Rpl38* expression. Values are means ± S.E., $n = 4$. In *C*, calvarial osteoblasts harvested from HES1 transgenics (HES1) and wild type littermate controls (WT) were co-cultured with splenocytes harvested from wild type mice, in the presence of 10 nM 1,25-dihydroxyvitamin D_3 (*Vit.D*; *black bars*) or control vehicle (*white bars*). Data are expressed as % of resorbed area. Values are means ± S.E., $n = 4–6$. *, significantly different from wild type cells, $p < 0.05$. + significantly different from cells treated with vehicle, $p < 0.05$.

male mice were not different from sex-matched littermate controls.

Hes1 Inactivation in Mature Osteoblasts Increases Bone Volume—For the conditional deletion of *Hes1* in mature osteoblasts, *Oc-Cre*/+;$Hes1^{loxP/loxP}$;$Hes3^{-/-}$;$Hes5^{-/-}$ mice were crossed with $Hes1^{loxP/loxP}$;$Hes3^{-/-}$;$Hes5^{-/-}$ mice to create *Oc-Cre*/+;$Hes1^{\Delta/\Delta}$;$Hes3^{-/-}$;$Hes5^{-/-}$ conditional null and $Hes1^{loxP/loxP}$;$Hes3^{-/-}$;$Hes5^{-/-}$ littermate controls. Recombination of $Hes1^{loxP}$ was documented by PCR analysis in calvarial DNA extracts from *Oc-Cre*/+;$Hes1^{\Delta/\Delta}$;$Hes3^{-/-}$;$Hes5^{-/-}$ mice (Fig. 4*A*). *Oc-Cre*/+;$Hes1^{\Delta/\Delta}$;$Hes3^{-/-}$;$Hes5^{-/-}$ mice appeared normal, contact radiography did not reveal skeletal abnormalities (data not shown), and there were no changes in weight, BMD, or femoral length when compared with littermate controls (Fig. 4*B*).

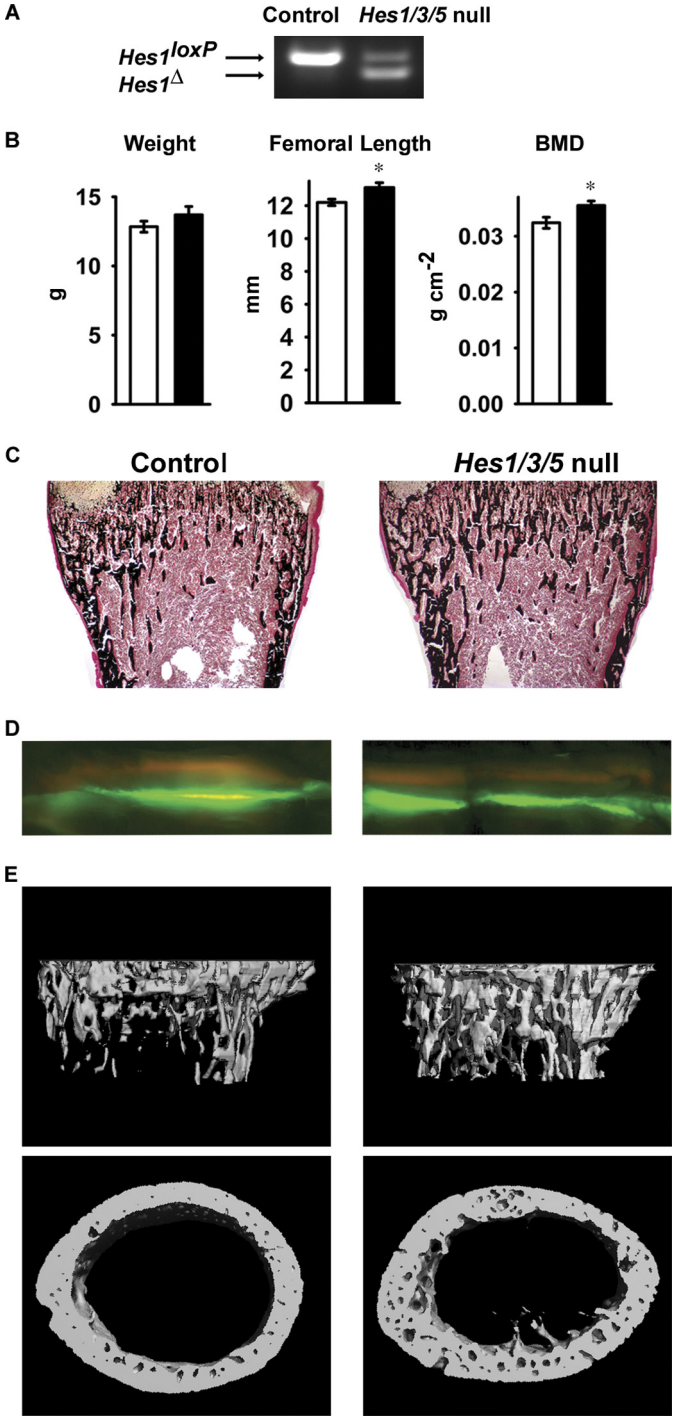

FIGURE 3. **Skeletal phenotype of 1-month-old male *Prx1-Cre*/+;$Hes1^{\Delta/\Delta}$;$Hes3^{-/-}$;$Hes5^{-/-}$ conditional null mice (*Hes1/3/5* null) and $Hes1^{loxP/loxP}$;$Hes3^{-/-}$;$Hes5^{-/-}$ littermate controls (Control) of the same sex.** In *A*, a representative PCR demonstrates the recombination of the $Hes1^{loxP}$ allele in calvarial DNA extracts. In *B*, the weight (g), femoral length (mm), and total BMD (g cm^{-2}) of *Prx1-Cre*/+;$Hes1^{\Delta/\Delta}$;$Hes3^{-/-}$;$Hes5^{-/-}$ mice (*black bars*) and controls (*white bars*) are shown. Values are means ± S.E., $n = 5–6$. *, significantly different from control mice, $p < 0.05$. *C* and *D*, von Kossa staining (*C*; final magnification, 40×) and calcein/demeclocycline labeling (*D*; final magnification, 100×) of representative femoral sections. Shown in *E* are micro-computed tomography of representative femurs.

The deletion of *Hes1* in mature osteoblasts caused an increase in trabecular bone volume in male mice, due to an increase in trabecular number that was observed from 1 to 6 months of age (Table 4 and Fig. 4*C*). In accordance with the

TABLE 3

Femoral histomorphometry and bone microarchitecture of 1-month-old *Prx1-Cre*/+;*Hes1*$^{\Delta/\Delta}$;*Hes3*$^{-/-}$;*Hes5*$^{-/-}$ (*Hes1/3/5* null) male mice and *Hes1*$^{loxP/loxP}$;*Hes3*$^{-/-}$;*Hes5*$^{-/-}$ controls

Femoral histomorphometry and microcomputed tomography were performed on femurs from 1-month-old *Prx1-Cre*/+;*Hes1*$^{\Delta/\Delta}$;*Hes3*$^{-/-}$;*Hes5*$^{-/-}$ male mice and *Hes1*$^{loxP/loxP}$;*Hes3*$^{-/-}$;*Hes5*$^{-/-}$ male littermate controls. Values are means ± S.E.; $n = 4–6$.

Males	Control	*Hes1/3/5* null
Histomorphometry		
Bone volume/tissue volume (%)	11.0 ± 1.3	18.8 ± 2.5[a]
Trabecular separation (μm)	199 ± 19	132 ± 25
Trabecular no. (mm^{-1})	4.6 ± 0.4	6.6 ± 0.7[a]
Trabecular thickness (μm)	23.5 ± 1.0	27.3 ± 1.5
Osteoblast surface/bone surface (%)	27.7 ± 1.9	30.8 ± 2.3
No. of osteoblasts/bone perimeter (mm^{-1})	27.1 ± 1.3	30.8 ± 2.6
Osteoid surface/bone surface (%)	4.6 ± 0.7	3.5 ± 0.6
Osteoclast surface/bone surface (%)	9.4 ± 1.1	9.6 ± 0.6
No. of osteoclasts/bone perimeter (mm^{-1})	4.5 ± 0.6	4.4 ± 0.3
Eroded surface/bone surface (%)	20.3 ± 2.6	20.4 ± 1.2
Mineral apposition rate ($\mu m\ day^{-1}$)	3.00 ± 0.23	2.67 ± 0.36
Mineralizing surface/bone surface (%)	1.2 ± 0.3	1.2 ± 0.3
Bone formation rate ($\mu m^2\ \mu m^{-3}\ day^{-1}$)	0.038 ± 0.011	0.030 ± 0.001
Microcomputed tomography		
Bone volume fraction (%)	9.7 ± 1.7	17.0 ± 2.5
Trabecular separation (μm)	286 ± 12	179 ± 26[a]
Trabecular no. (mm^{-1})	3.6 ± 0.2	5.8 ± 0.7[a]
Trabecular thickness (μm)	40 ± 1	39 ± 1
Connectivity density (mm^{-3})	148.6 ± 34.5	355.4 ± 65.5[a]
Structure model index	2.09 ± 0.17	1.81 ± 0.14
Cortical thickness (μm)	107 ± 5	97 ± 6

[a] Significantly different from controls, $p < 0.05$.

results obtained from the conditional deletion of *Hes1* in the limb bud, female mice did not exhibit a skeletal phenotype (data not shown). Osteoblast number was not changed and *Oc-Cre*/+;*Hes1*$^{\Delta/\Delta}$;*Hes3*$^{-/-}$;*Hes5*$^{-/-}$ male mice displayed a transient increase in mineral apposition rate at 1 month of age, followed by a transient decrease at 3 months of age (Table 4 and Fig. 4*D*). In accordance with the results observed in HES1 male transgenics, the number of osteoclasts was decreased in *Oc-Cre*/+;*Hes1*$^{\Delta/\Delta}$;*Hes3*$^{-/-}$;*Hes5*$^{-/-}$ mice at 1 month of age. This indicates that the deletion of *Hes1* in osteoblasts affects osteoclast number and possibly function, because there was a tendency toward decreased eroded surface (Table 4). Confirming the histomorphometric findings, microcomputed tomography revealed increased trabecular bone volume, number, and connectivity density in *Oc-Cre*/+;*Hes1*$^{\Delta/\Delta}$;*Hes3*$^{-/-}$;*Hes5*$^{-/-}$ mice. The structural model index was closer to zero, demonstrating a preponderance of plate-like trabecular structures (Table 4; Fig. 4*E*). *Oc-Cre*/+;*Hes1*$^{\Delta/\Delta}$;*Hes3*$^{-/-}$;*Hes5*$^{-/-}$ mice exhibited a modest decrease in cortical thickness at 6 months of age (Table 4 and Fig. 4*E*). These results indicate that inactivation of *Hes1* affects the cortical bone compartment by inducing an age-related loss in cortical thickness.

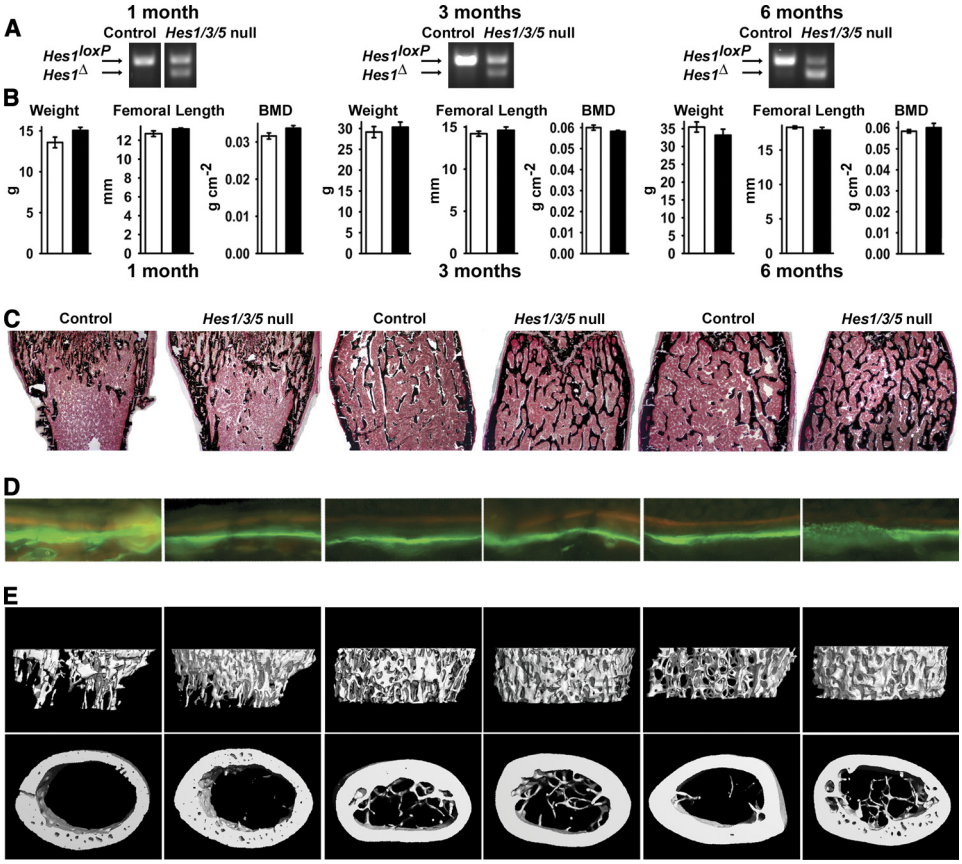

FIGURE 4. **Skeletal phenotype of 1 month (*left*), 3 month (middle) and 6 month (*right*) old male *Oc-Cre*/+;*Hes1*$^{\Delta/\Delta}$;*Hes3*$^{-/-}$;*Hes5*$^{-/-}$ conditional null mice (*Hes1/3/5* null) and *Hes1*$^{loxP/loxP}$;*Hes3*$^{-/-}$;*Hes5*$^{-/-}$ littermate controls (Control) of the same sex.** *A*, representative PCR demonstrates the recombination of the *Hes1*^{loxP} allele in calvarial DNA extracts. *B*, the weight (g), femoral length (mm), and total BMD (g cm^{-2}) of *Oc-Cre*/+;*Hes1*$^{\Delta/\Delta}$;*Hes3*$^{-/-}$;*Hes5*$^{-/-}$ mice (*black bars*) and controls (*white bars*). *C* and *D*, von Kossa staining (*C*; final magnification, 40×) and calcein/demeclocycline labeling (*D*; final magnification, 100×) of representative femoral sections. *E*, microcomputed tomography of representative femurs.

TABLE 4

Femoral histomorphometry and bone microarchitecture of 1-, 3-, and 6-month-old *Oc-Cre*/+;*Hes1*$^{\Delta/\Delta}$;*Hes3*$^{-/-}$;*Hes5*$^{-/-}$ (Hes1/3/5 null) male mice and *Hes1*$^{loxP/loxP}$;*Hes3*$^{-/-}$;*Hes5*$^{-/-}$ (Control) controls

Femoral histomorphometry and microcomputed tomography were performed on femurs from 1-, 3-, and 6-month-old *Oc-Cre*/+;*Hes1*$^{\Delta/\Delta}$;*Hes3*$^{-/-}$;*Hes5*$^{-/-}$ male mice and *Hes1*$^{loxP/loxP}$;*Hes3*$^{-/-}$;*Hes5*$^{-/-}$ male littermate controls. Values are means ± S.E.; $n = 5–12$.

Males	1-month-old		3-month-old		6-month-old	
	Control	*Hes1/3/5* null	Control	*Hes1/3/5* null	Control	*Hes1/3/5* null
Femoral histomorphometry						
Bone volume/tissue volume (%)	9.5 ± 2.0	16.7 ± 2.2[a]	18.2 ± 1.3	25.1 ± 0.9[a]	16.4 ± 1.2	27.9 ± 4.0[a]
Trabecular separation (μm)	282 ± 98	142 ± 26	135 ± 8	97 ± 5[a]	175 ± 9	115 ± 18[a]
Trabecular no. (mm^{-1})	4.1 ± 0.8	6.5 ± 0.9	6.1 ± 0.3	7.8 ± 0.3[a]	4.9 ± 0.2	6.8 ± 0.6[a]
Trabecular thickness (μm)	22.9 ± 0.7	25.8 ± 0.6[a]	29.9 ± 1.1	32.5 ± 1.0	33.5 ± 1.8	40.1 ± 4.0
Osteoblast surface/bone surface (%)	14.8 ± 1.7	18.7 ± 4.0	6.5 ± 0.4	6.3 ± 0.8	9.2 ± 0.6	8.3 ± 1.4
No. of osteoblasts/bone perimeter (mm^{-1})	13.8 ± 1.5	17.0 ± 3.9	6.7 ± 0.4	6.5 ± 0.7	9.7 ± 0.7	8.9 ± 1.4
Osteoid surface/bone surface (%)	1.88 ± 0.40	1.08 ± 0.33	0.17 ± 0.07	0.20 ± 0.07	0.16 ± 0.05	0.07 ± 0.03
Osteoclast surface/bone surface (%)	12.0 ± 1.0	10.0 ± 0.6	7.5 ± 0.6	7.2 ± 0.5	9.4 ± 0.5	8.5 ± 0.6
No. of osteoclasts/bone perimeter (mm^{-1})	5.8 ± 0.5	4.6 ± 0.3[a]	3.4 ± 0.2	3.2 ± 0.2	4.0 ± 0.2	3.7 ± 0.2
Eroded surface/bone surface (%)	25.0 ± 1.9	20.6 ± 1.4	14.6 ± 1.1	13.6 ± 0.8	16.3 ± 0.9	15.3 ± 0.9
Mineral apposition rate (μm day^{-1})	1.44 ± 0.09	1.95 ± 0.10[a]	0.62 ± 0.04	0.50 ± 0.04[a]	0.50 ± 0.06	0.49 ± 0.03
Mineralizing surface/bone surface (%)	3.1 ± 0.2	2.4 ± 0.5	4.6 ± 1.0	2.8 ± 0.6	5.0 ± 1.5	5.1 ± 1.3
Bone formation rate ($\mu m^2\ \mu m^{-3}\ day^{-1}$)	0.045 ± 0.006	0.043 ± 0.006	0.031 ± 0.007	0.014 ± 0.004[a]	0.030 ± 0.010	0.026 ± 0.007
Microcomputed tomography						
Bone volume fraction (%)	10.8 ± 1.9	16.7 ± 1.8[a]	16.5 ± 0.9	26.0 ± 1.5[a]	14.6 ± 2.8	26.9 ± 1.8[a]
Trabecular separation (μm)	341 ± 67	195 ± 16	176 ± 8	137 ± 6[a]	222 ± 17	155 ± 7[a]
Trabecular no. (mm^{-1})	3.6 ± 0.6	5.3 ± 0.4[a]	5.4 ± 0.2	6.5 ± 0.2[a]	4.4 ± 0.4	5.8 ± 0.2[a]
Trabecular thickness (μm)	40 ± 1	41 ± 1	43 ± 1	46 ± 2	50 ± 2	53 ± 3
Connectivity density (mm^{-3})	200 ± 49	361 ± 45[a]	247 ± 22	385 ± 30[a]	149 ± 25	273 ± 14[a]
Structure model index	1.87 ± 0.05	1.73 ± 0.14	1.7 ± 0.1	0.9 ± 0.2[a]	1.97 ± 0.18	0.80 ± 0.29[a]
Cortical thickness (μm)	118 ± 6	115 ± 4	223 ± 11	212 ± 4	229 ± 13	188 ± 11[a]

[a] Significantly different from wild type controls, $p < 0.05$.

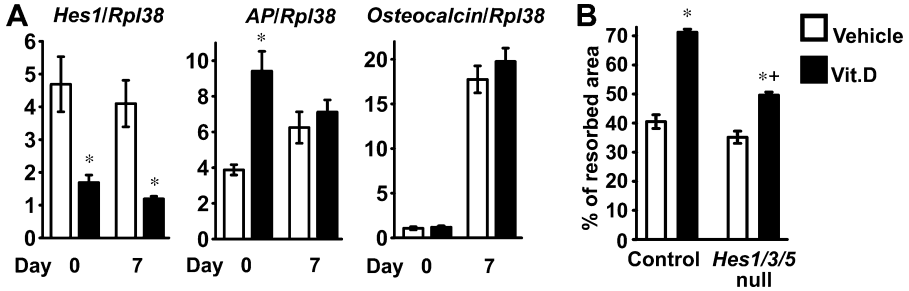

FIGURE 5. **Consequences of *Hes1* inactivation on osteoblastic function *in vitro*.** In panel *A*, Calvarial osteoblasts were harvested from *Oc-Cre*/+;*Hes1*$^{\Delta/\Delta}$;*Hes3*$^{-/-}$;*Hes5*$^{-/-}$ conditional null mice (black bars) and *Hes1*$^{loxP/loxP}$;*Hes3*$^{-/-}$;*Hes5*$^{-/-}$ littermate controls (white bars). Total RNA was extracted at confluence and after 7 days of culture in conditions favoring osteoblastogenesis; mRNA was reverse-transcribed and amplified by real time RT-PCR in the presence of specific primers. Data are expressed as *Hes1*, alkaline phosphatase (*Ap*), and osteocalcin copy number, determined by real time RT-PCR, corrected for *Rpl38* expression. Values are means ± S.E., $n = 4$. *, significantly different from control cells, $p < 0.05$. In *B*, calvarial osteoblasts harvested from *Oc-Cre*/+;*Hes1*$^{\Delta/\Delta}$;*Hes3*$^{-/-}$;*Hes5*$^{-/-}$ conditional null mice (*Hes1/3/5* null) and *Hes1*$^{loxP/loxP}$;*Hes3*$^{-/-}$;*Hes5*$^{-/-}$ littermate controls (Control) were co-cultured with splenocytes harvested from wild type mice, in the presence of 10 nM 1,25-dihydroxyvitamin D_3 (*Vit.D, black bars*) or control vehicle (*white bars*). Data are expressed as % of resorbed area. Values are means ± S.E., $n = 4–6$. *, significantly different from control cells, $p < 0.05$. +, significantly different from cells treated with vehicle, $p < 0.05$.

Hes1 Regulates Osteoblastogenesis and Osteoclastogenesis in Vitro—To study the mechanisms responsible for the consequences of *Hes1* inactivation, the differentiation of calvarial osteoblasts from *Oc-Cre*/+;*Hes1*$^{\Delta/\Delta}$;*Hes3*$^{-/-}$;*Hes5*$^{-/-}$ conditional null or *Hes1*$^{loxP/loxP}$;*Hes3*$^{-/-}$;*Hes5*$^{-/-}$ littermate controls of both sexes was analyzed. *Hes1* mRNA levels were decreased in confluent cultures and in cells maintained in differentiation medium for 7 days, and alkaline phosphatase transcripts levels were induced upon down-regulation of *Hes1* in confluent cultures (Fig. 5*A*). However, osteocalcin transcripts (Fig. 5*A*) and levels of alkaline phosphatase activity and mineralization of the culture were not increased (data not shown).

To determine whether inactivation of *Hes1* in osteoblasts impaired osteoclast formation and function, calvarial osteoblasts from *Oc-Cre*/+;*Hes1*$^{\Delta/\Delta}$;*Hes3*$^{-/-}$;*Hes5*$^{-/-}$ conditional null or *Hes1*$^{loxP/loxP}$;*Hes3*$^{-/-}$;*Hes5*$^{-/-}$ littermate controls of both sexes were co-cultured with splenocytes from wild type FVB mice. Under basal conditions, resorption was not different between experimental and control cultures. Treatment with 1,25-dihydroxyvitamin D_3 enhanced resorption in control cultures, and this effect was blunted in co-cultures of *Hes1* conditional null osteoblasts (Fig. 5*B*). This is in agreement with the suppressed number of osteoclasts and eroded surface observed in male *Hes1* conditional null mice.

DISCUSSION

In the present study, we demonstrate that *Hes1* modulates bone remodeling, as perturbing its expression in osteoblastic cells results in significant alterations in cancellous bone volume and microarchitecture. Transgenic mice overexpressing HES1 under the control of the 3.6-kb *Col1a1* promoter display impaired growth and shortened life span. This could be due to excessive dosage of HES1 in extraskeletal tissues, be-

cause expression of the 3.6-kb *Col1a1* promoter fragment is not entirely specific to skeletal cells (36). HES1 transgenic mice were moderately osteopenic and whereas males exhibited increased bone resorption, females displayed a reduced number of osteoblasts. These differences could be explained by different degrees of penetrance of the *Hes1* transgene in the two sexes or by a sexually dimorphic mechanism of HES1 action in the skeleton. *In vitro* studies of osteoblastic differentiation of transgenic cells confirmed that HES1 suppressed osteoblastogenesis, and by acting on osteoblastic cells, it increased bone resorption. These results are in accordance with the inhibitory effects of HES1 on osteocalcin expression in osteoblastic cells and explain the osteopenic phenotype observed in HES1 transgenics (27).

The consequences of the conditional inactivation of *Hes1* were analyzed in the context of the global deletion of *Hes3* and *Hes5*. Although HES3 and HES5 are expressed in osteoblasts, $Hes3^{-/-}$;$Hes5^{-/-}$ mice had no skeletal phenotype, suggesting that these genes are dispensable for normal skeletal development and bone remodeling, and their functions may be carried out by HES1. Inactivation of *Hes1* in the limb bud or in mature osteoblasts caused a skeletal phenotype only in male mice, and this may be explained by earlier studies demonstrating sexual dimorphism in murine skeletal maturation and trabecular microarchitecture (56, 57). We could not detect differences in the recombination of the $Hes1^{loxP}$ allele between male and female *Hes1* conditional null mice (data not shown); therefore, it is unlikely that Cre recombination was more efficient in skeletal cells from male than from female mice.

Even though inactivation of *Hes1* in the limb bud increased the number and connectivity of trabeculae, osteoblast number and function were not changed. These observations are consistent with an inhibitory effect of HES1 on chondrogenesis and suggest that *Hes1* impairs endochondral bone formation (58). This observation also is in accordance with the suppression of collagen type 2 α1 transcription by HES1 (58). Studies on the conditional inactivation of *Hes1* in a *Hes5* null background have suggested that HES1 and HES5 are dispensable for cartilage development (59). This discrepancy with our results could be explained by the fact that the phenotypic analysis was conducted in mice with a functional *Hes3* allele, which could have compensated for the loss of *Hes1* and *Hes5*.

Inactivation of *Hes1* in mature osteoblasts caused a dramatic increase in trabecular bone volume and in the structural properties of cancellous bone, favoring the formation of plate-like trabecular structures and increasing connectivity. Although the phenotype of the *Hes1* inactivation in the skeleton was striking, the mechanisms responsible were less evident. The increased bone volume observed seemed to be secondary to a transient increase in osteoblast function and a decrease in osteoclast function. It is of interest that despite the fact that functional changes were short-lived, the consequences were long lasting and observed up to 6 months of age. Cellular experiments confirmed an increase in osteoblast function and a decrease in the resorptive capacity of osteoclast precursors exposed to *Hes1* null osteoblasts. Although the effects were relatively modest, they provide an explanation for the phenotype observed *in vivo*.

Although *Hes1* is a target of Notch signaling in osteoblasts, the phenotype observed in these studies indicates that the misexpression of HES1 does not phenocopy that of Notch. HES1 transgenics exhibit a less pronounced skeletal phenotype than mice overexpressing the Notch1 intracellular domain under the control of the 3.6-kb *Col1a1* promoter (23). Conditional inactivation of *Hes1* in the limb bud caused a modest phenotype, whereas inactivation of *Notch1* and *Notch2* in the limb bud resulted in severe skeletal malformations due to abnormal accumulation of hypertrophic chondrocytes (22). An analogous phenotype to the *Notch1* and *Notch2* inactivation in the limb bud was observed following the conditional inactivation of Epstein-Barr virus latency C promoter binding factor 1, suppressor of Hairless and Lag-1 (*Csl*) in chondrocytes (60). CSL forms a complex with the Notch intracellular domain to induce transcription of Notch target genes in the canonical Notch signaling pathway (9). These observations would confirm a distinct function of Notch canonical signaling in skeletal development that cannot be fully accounted for by its induction of HES1 expression. This would suggest that other Notch target genes, such as *Hey1*, *Hey2*, and *HeyL* may be responsible, at least in part, for the effects of Notch in the skeleton. The distinct function of *Hes1* is further substantiated by studies demonstrating that the conditional inactivation of *Notch1* and *Notch2* in mature osteoblasts causes no alteration in osteoblastic function, whereas the inactivation of *Hes1* causes a distinct phenotype (22). *In vivo* and *in vitro* studies have revealed that in contrast to the stimulatory effects of *Hes1* on osteoclast function, Notch suppresses osteoclastogenesis (21, 34, 35). These observations demonstrate that the skeletal effects of HES1 in osteoblasts are largely independent from those of Notch signaling (21, 34, 35). It is also important to note that the expression of *Hes1* in skeletal cells is regulated by alternative signals, such as connective tissue growth factor, which induces *Hes1* by mechanisms independent from Notch transactivation (24).

Osteoporosis, a disease characterized by reduction in bone mass, is a major health care problem due to the large number of people affected and the morbidity and mortality associated with osteoporotic fractures (15, 61). We have demonstrated that inactivation of *Hes1*, *Hes3*, and *Hes5* not only increases bone mass but also enhances the microarchitectural properties of the skeleton. Although inhibition of intracellular protein function is difficult to achieve, targeted down-regulation of *Hes1* expression or activity in osteoblasts could be considered as a possible strategy in the development of novel therapies for osteoporosis. Intracellular and extracellular inhibition of Notch signaling has been proposed for the treatment of a variety of disorders, such as Alzheimer disease and malignancies, and similar approaches could be considered for the inactivation of *Hes1* (62). In conclusion, HES1 suppresses osteoblast function and enhances bone resorption and, as a consequence, regulates bone mass and bone microarchitecture.

Acknowledgments—We thank Drs. R. Kageyama for the Hes1$^{loxP/loxP}$, Hes3$^{-/-}$, and Hes5$^{-/-}$ mice, T. Clemens for osteocalcin-Cre transgenic mice, J. B. Lian for osteocalcin cDNA, and J. A. Lorenzo for helpful discussions. The authors thank A. Kent, K. Parker, and M. Monarca for technical help and M. Yurczak for secretarial assistance.

REFERENCES

1. Iso, T., Kedes, L., and Hamamori, Y. (2003) *J. Cell. Physiol.* **194,** 237–255
2. Katoh, M., and Katoh, M. (2004) *Int. J. Oncol.* **25,** 529–534
3. Kageyama, R., Ohtsuka, T., and Kobayashi, T. (2007) *Development* **134,** 1243–1251
4. Fischer, A., and Gessler, M. (2007) *Nucleic Acids Res.* **35,** 4583–4596
5. Cornell, R. A., and Eisen, J. S. (2005) *Semin. Cell Dev. Biol.* **16,** 663–672
6. Androutsellis-Theotokis, A., Leker, R. R., Soldner, F., Hoeppner, D. J., Ravin, R., Poser, S. W., Rueger, M. A., Bae, S. K., Kittappa, R., and McKay, R. D. (2006) *Nature* **442,** 823–826
7. Gridley, T. (2007) *Development* **134,** 2709–2718
8. Lee, J., Basak, J. M., Demehri, S., and Kopan, R. (2007) *Development* **134,** 2795–2806
9. Zanotti, S., and Canalis, E. (2010) *Mol. Cell. Biol.* **30,** 886–896
10. Murtaugh, L. C., Stanger, B. Z., Kwan, K. M., and Melton, D. A. (2003) *Proc. Natl. Acad. Sci. U.S.A.* **100,** 14920–14925
11. Kodama, Y., Hijikata, M., Kageyama, R., Shimotohno, K., and Chiba, T. (2004) *Gastroenterology* **127,** 1775–1786
12. Hatakeyama, J., Bessho, Y., Katoh, K., Ookawara, S., Fujioka, M., Guillemot, F., and Kageyama, R. (2004) *Development* **131,** 5539–5550
13. van Es, J. H., van Gijn, M. E., Riccio, O., van den Born, M., Vooijs, M., Begthel, H., Cozijnsen, M., Robine, S., Winton, D. J., Radtke, F., and Clevers, H. (2005) *Nature* **435,** 959–963
14. Ishibashi, M., Ang, S. L., Shiota, K., Nakanishi, S., Kageyama, R., and Guillemot, F. (1995) *Genes Dev.* **9,** 3136–3148
15. Canalis, E., Giustina, A., and Bilezikian, J. P. (2007) *N. Engl. J. Med.* **357,** 905–916
16. Canalis, E. (2005) *N. Engl. J. Med.* **352,** 2014–2016
17. Bianco, P., and Gehron Robey, P. (2000) *J. Clin. Invest.* **105,** 1663–1668
18. Canalis, E., Economides, A. N., and Gazzerro, E. (2003) *Endocr. Rev.* **24,** 218–235
19. Westendorf, J. J., Kahler, R. A., and Schroeder, T. M. (2004) *Gene* **341,** 19–39
20. Canalis, E. (2008) *Sci. Signal.* **1,** pe17
21. Engin, F., Yao, Z., Yang, T., Zhou, G., Bertin, T., Jiang Chen, Y., Wang, L., Zheng, H., Sutton, R. E., Boyce, B. F., and Lee, B. (2008) *Nat. Med.* **14,** 299–305
22. Hilton, M. J., Tu, X., Wu, X., Bai, S., Zhao, H., Kobayashi, T., Kronenberg, H. M., Teitelbaum, S. L., Ross, F. P., Kopan, R., and Long, F. (2008) *Nat. Med.* **14,** 306–314
23. Zanotti, S., Smerdel-Ramoya, A., Stadmeyer, L., Durant, D., Radtke, F., and Canalis, E. (2008) *Endocrinology* **149,** 3890–3899
24. Smerdel-Ramoya, A., Zanotti, S., Deregowski, V., and Canalis, E. (2008) *J. Biol. Chem.* **283,** 22690–22699
25. Ross, D. A., Rao, P. K., and Kadesch, T. (2004) *Mol. Cell. Biol.* **24,** 3505–3513
26. Ross, D. A., Hannenhalli, S., Tobias, J. W., Cooch, N., Shiekhattar, R., and Kadesch, T. (2006) *Mol. Endocrinol.* **20,** 698–705
27. Zhang, Y., Lian, J. B., Stein, J. L., van Wijnen, A. J., and Stein, G. S. (2009) *J. Cell. Biochem.* **108,** 651–659
28. Shen, Q., and Christakos, S. (2005) *J. Biol. Chem.* **280,** 40589–40598
29. McLarren, K. W., Lo, R., Grbavec, D., Thirunavukkarasu, K., Karsenty, G., and Stifani, S. (2000) *J. Biol. Chem.* **275,** 530–538
30. Lee, J. S., Thomas, D. M., Gutierrez, G., Carty, S. A., Yanagawa, S., and Hinds, P. W. (2006) *J. Bone Miner Res.* **21,** 921–933
31. Suh, J. H., Lee, H. W., Lee, J. W., and Kim, J. B. (2008) *Biochem. Biophys. Res. Commun.* **367,** 97–102
32. Lacey, D. L., Timms, E., Tan, H. L., Kelley, M. J., Dunstan, C. R., Burgess, T., Elliott, R., Colombero, A., Elliott, G., Scully, S., Hsu, H., Sullivan, J., Hawkins, N., Davy, E., Capparelli, C., Eli, A., Qian, Y. X., Kaufman, S., Sarosi, I., Shalhoub, V., Senaldi, G., Guo, J., Delaney, J., and Boyle, W. J. (1998) *Cell* **93,** 165–176
33. Teitelbaum, S. L. (2007) *Am. J. Pathol.* **170,** 427–435
34. Yamada, T., Yamazaki, H., Yamane, T., Yoshino, M., Okuyama, H., Tsuneto, M., Kurino, T., Hayashi, S., and Sakano, S. (2003) *Blood* **101,** 2227–2234
35. Bai, S., Kopan, R., Zou, W., Hilton, M. J., Ong, C. T., Long, F., Ross, F. P., and Teitelbaum, S. L. (2008) *J. Biol. Chem.* **283,** 6509–6518
36. Kalajzic, I., Kalajzic, Z., Kaliterna, M., Gronowicz, G., Clark, S. H., Lichtler, A. C., and Rowe, D. (2002) *J. Bone Miner. Res.* **17,** 15–25
37. Irwin, N. (1989) in *Sambrook* (Fritsch, E. F., and Maniatis, T., eds) pp. 9.32–9.36, Cold Spring Harbor Laboratory Press, New York
38. Imayoshi, I., Shimogori, T., Ohtsuka, T., and Kageyama, R. (2008) *Development* **135,** 2531–2541
39. Hirata, H., Tomita, K., Bessho, Y., and Kageyama, R. (2001) *EMBO J.* **20,** 4454–4466
40. Cau, E., Gradwohl, G., Casarosa, S., Kageyama, R., and Guillemot, F. (2000) *Development* **127,** 2323–2332
41. Logan, M., Martin, J. F., Nagy, A., Lobe, C., Olson, E. N., and Tabin, C. J. (2002) *Genesis.* **33,** 77–80
42. Zhang, M., Xuan, S., Bouxsein, M. L., von Stechow, D., Akeno, N., Faugere, M. C., Malluche, H., Zhao, G., Rosen, C. J., Efstratiadis, A., and Clemens, T. L. (2002) *J. Biol. Chem.* **277,** 44005–44012
43. Nagy, T. R., Prince, C. W., and Li, J. (2001) *J. Bone Miner. Res.* **16,** 1682–1687
44. Gazzerro, E., Pereira, R. C., Jorgetti, V., Olson, S., Economides, A. N., and Canalis, E. (2005) *Endocrinology* **146,** 655–665
45. Parfitt, A. M., Drezner, M. K., Glorieux, F. H., Kanis, J. A., Malluche, H., Meunier, P. J., Ott, S. M., and Recker, R. R. (1987) *J. Bone Miner. Res.* **2,** 595–610
46. Bouxsein, M. L., Boyd, S. K., Christiansen, B. A., Guldberg, R. E., Jepsen, K. J., and Müller, R. (2010) *J Bone Miner Res.* **25,** 1468–1486
47. McCarthy, T. L., Centrella, M., and Canalis, E. (1990) *J. Biol. Chem.* **265,** 15353–15356
48. Takahashi, N., Akatsu, T., Udagawa, N., Sasaki, T., Yamaguchi, A., Moseley, J. M., Martin, T. J., and Suda, T. (1988) *Endocrinology* **123,** 2600–2602
49. Wyzga, N., Varghese, S., Wikel, S., Canalis, E., and Sylvester, F. A. (2004) *Bone* **35,** 614–620
50. Lee, S. K., Kalinowski, J., Jastrzebski, S., and Lorenzo, J. A. (2002) *J. Immunol.* **169,** 2374–2380
51. Nazarenko, I., Pires, R., Lowe, B., Obaidy, M., and Rashtchian, A. (2002) *Nucleic Acids Res.* **30,** 2089–2195
52. Nazarenko, I., Lowe, B., Darfler, M., Ikonomi, P., Schuster, D., and Rashtchian, A. (2002) *Nucleic Acids Res.* **30,** e37
53. Akazawa, C., Sasai, Y., Nakanishi, S., and Kageyama, R. (1992) *J. Biol. Chem.* **267,** 21879–21885
54. Lian, J., Stewart, C., Puchacz, E., Mackowiak, S., Shalhoub, V., Collart, D., Zambetti, G., and Stein, G. (1989) *Proc. Natl. Acad. Sci. U.S.A.* **86,** 1143–1147
55. Kouadjo, K. E., Nishida, Y., Cadrin-Girard, J. F., Yoshioka, M., and St-Amand, J. (2007) *BMC Genomics* **8,** 127
56. Glatt, V., Canalis, E., Stadmeyer, L., and Bouxsein, M. L. (2007) *J. Bone Miner. Res.* **22,** 1197–1207
57. DeMambro, V. E., Clemmons, D. R., Horton, L. G., Bouxsein, M. L., Wood, T. L., Beamer, W. G., Canalis, E., and Rosen, C. J. (2008) *Endocrinology* **149,** 2051–2061
58. Grogan, S. P., Olee, T., Hiraoka, K., and Lotz, M. K. (2008) *Arthritis Rheum.* **58,** 2754–2763
59. Karlsson, C., Brantsing, C., Kageyama, R., and Lindahl, A. (2010) *Cells Tissues Organs* **192,** 17–27
60. Mead, T. J., and Yutzey, K. E. (2009) *Proc. Natl. Acad. Sci. U.S.A.* **106,** 14420–14425
61. Looker, A. C., Orwoll, E. S., Johnston, C. C., Jr., Lindsay, R. L., Wahner, H. W., Dunn, W. L., Calvo, M. S., Harris, T. B., and Heyse, S. P. (1997) *J. Bone Miner. Res.* **12,** 1761–1768
62. Moellering, R. E., Cornejo, M., Davis, T. N., Del Bianco, C., Aster, J. C., Blacklow, S. C., Kung, A. L., Gilliland, D. G., Verdine, G. L., and Bradner, J. E. (2009) *Nature* **462,** 182–188